Energy & Buildings 173 (2018) 678–688

Contents lists available at ScienceDirect

Energy & Buildings

journal homepage: www.elsevier.com/locate/enbuild

Thermal performance and numerical simulation of geopolymer concrete containing different types of thermoregulating materials for passive building applications

Vinh Duy Cao[a,b], Shima Pilehvar[a,c], Carlos Salas-Bringas[b], Anna M. Szczotok[a,d], Tri Quang Bui[a], Manuel Carmona[d], Juan F. Rodriguez[d], Anna-Lena Kjøniksen[a,*]

[a] Faculty of Engineering, Østfold University College, Halden N-1757, Norway
[b] Faculty of Science and Technology, Norwegian University of Life Sciences, Ås N-1432, Norway
[c] Department of Material Engineering and Manufacturing, Technical University of Cartagena, Cartagena, Murcia, Spain
[d] Department of Chemical Engineering, University of Castilla – La Mancha, Ciudad Real 13004, Spain

ARTICLE INFO

Article history:
Received 6 December 2017
Revised 26 February 2018
Accepted 7 June 2018
Available online 20 June 2018

Keywords:
Microencapsulated phase change materials
Geopolymer concrete
Thermal performance
Implicit method
Finite differences

ABSTRACT

Geopolymer concrete (GPC) containing microencapsulated phase change materials (MPCM) were fabricated in order to achieve a high thermal energy storage capacity of an environmental friendly concrete. Different kinds of MPCM were utilized to investigate the influence of the hygroscopic nature, latent heat, and size of microcapsules on the microstructure and thermal properties of GPC. A combination of polar functional groups on the polymer shell and microcapsules with a small size was found to improve the interface bonds between microcapsules and the GPC matrix, how well the MPCM is dispersed in the GPC, and the thermal insulation properties of the GPC. The energy storage capacity of GPC increases at higher concentrations of MPCM and with a higher latent heat of the MPCM. To determine the thermal impact of buildings utilizing GPC containing MPCM, a numerical model was utilized. The model is based on the implicit finite differences method using an energy balance approach and the heat capacity method. In order to improve the model, a new equation was successfully utilized to fit the specific heat capacity of GPC containing MPCM as function of temperature. The numerical model was verified by experimental measurements of the thermal performance of the GPC. The simulated numerical values obtained for GPC containing MPCM were in good agreement with the experimental data. Higher amounts of MPCM and thicker concrete walls reduce the power consumption needed to maintain an indoor temperature of 23 °C. A power reduction of nearly 35% was achieved when utilizing a 75 mm concrete wall containing 5.2 wt.% MPCM. These building materials are therefore promising for improving human comfort and for reducing the energy consumption of buildings.

1. Introduction

A promising solution for reducing indoor temperature fluctuations, maintaining thermal comfort, and minimizing the peak of the cooling and heating loads is integration of microencapsulated phase change materials (MPCM) in building materials. This will enhance the heat storage capacity during the phase transition of the phase change materials and reduce the thermal conductivity of the building materials. Portland cement concrete is among the best known materials for integration of MPCM due to the high mechanical strength and the possibility of changing the properties by varying the concrete recipe [1–9]. However, the main drawback of producing Portland cement is the CO_2 emission, which contributes to about 5–8% of the total CO_2 emissions, and is the third man-made CO_2 source after transport and energy generation [10]. Accordingly, it is advantageous to use green materials to partly replace Portland cement concrete. Geopolymer synthesized by alkali activation of aluminosilicate materials in amorphous form (from industrial waste) is environmentally friendly [11,12]. Replacing Portland cement by geopolymer as the main concrete binder can significantly reduce the CO_2 emission from the cement industry. Although geopolymer concrete containing microencapsulated phase change materials is very interesting, research regarding

* Corresponding author.
E-mail address: anna.l.kjoniksen@hiof.no (A.-L. Kjøniksen).

https://doi.org/10.1016/j.enbuild.2018.06.011

Table 1
The fundamental data of the microencapsulated phase change materials.

MPCM name	Hygroscopic nature of shell	Size (μm)		T_{melt}(°C)	ΔH(J/g)	Core/Shell ratio	Ref
		Single	Aggregates (mean size)				
PS-DVB/RT27	nonpolar groups	10–100	130	24.9	100	11:9	[25]
MF/PCM24	polar groups	10–30	21	21.9	154	9:1	[26]

these materials is limited [3,5]. In addition, previous publications have mainly been investigating the effect of one type of microcapsules [1–7]. There are very few investigations comparing different types of microcapsules to examine the effect of the polarity of the polymer shell, as well as the size and the heat storage capacity of the microcapsules.

It is helpful to utilize numerical models to estimate the thermal impact of geopolymer concrete containing MPCM in buildings. Some numerical methods have been developed to simulate the effect of heat transfer during the solid–liquid phase change. These are the temperature transforming model, the heat source method, the enthalpy method and the heat capacity method [13–18]. One of the most commonly used numerical methods is the heat capacity method [16–18]. For this method a good agreement between experimental data and the numerical methods are found. Nevertheless, this method defines the apparent specific heat capacity as a stepwise function of temperature, which exhibits a discontinuity of the specific heat capacity at the start and end of the melting point range. This can produce a mismatch between the model and realistic conditions. Furthermore, most studies assume that the melting peak is symmetric, and define $C_p(T)$ as a piecewise function of temperature [16,17] or a Gaussian function of temperature [19]. However, for concrete containing microcapsules this assumption is not in agreement with the experimental curve of $C_p(T)$, which exhibit an asymmetric melting peak [3,20–22].

Previously, it was found that agglomeration of the microcapsules have an important effect on the properties of geopolymer concrete [3]. Accordingly, the current work utilizes microencapsulated phase change materials that do not form large agglomerates. Unlike the previous study [3], two types of microcapsules with different polymer shells, heat storage capacity and sizes were utilized to explore their influence on the microstructure and thermal properties of geopolymer concrete. In addition, a simple equation is developed to reproduce the heat capacity for GPC containing microencapsulated phase change materials. This equation was utilized in the numerical model to predict the thermal impact of GPC containing MPCM. Finally, a simple experimental system was designed to verify the performance of the numerical model. Previous studies have compared the thermal impact based on numerical calculations with experimental results for Portland cement plastering mortars containing MPCM [23,24]. There is however a lack of studies where this kind of comparison have been conducted on concretes or geopolymer materials containing MPCM.

2. Experimental

2.1. Materials

Two different kinds of microcapsules were utilized:

- PS-DVB/RT27 microcapsules consists of a paraffin Rubitherm®RT27 core coated with a PS-DVB (polystyrene cross-linked with divinylbenzene) shell. These microcapsules were made by a polymerization suspension process in our lab [25].
- Commercial Microtek MPCM24D (MF/PCM24) which contains a paraffin core and a melamine-formaldehyde polymer shell (MF).

The properties of the microcapsules are summarized in Table 1.

Table 2 summarizes the composition of geopolymer concrete containing MPCM (MPCM-GPC). The main components of the geopolymer concrete are sand (Gunnar Holth and Skolt Pukkverk AS, Norway), aggregates (Gunnar Holth and Skolt Pukkverk AS, Norway), fly ash (FA) (Norcem, Germany), ground granulated blast furnace slag (GGBFS) (Cemex, Germany), retarder (FLUBE OS 39, Bozzetto Group, Italy), an alkaline activator solution and microcapsules. The alkaline activator solution is a mixture of a sodium silicate solution Na_2SiO_3 (35 wt.% solid) and 14 M sodium hydroxide NaOH (560 g/L). Based on a previous study [27], the mixing ratio between Na_2SiO_3 and NaOH is 1.5 corresponding to $m_{Na2SiO3(aq)} = 120$ g, and $m_{NaOH(aq)} = 80$ g. MPCM was mixed into the GPC as the final mixing step to minimize the shear forces on the microcapsules during the mixing process. For more information about the recipe and the mixing process, see Pilehvar et al. [5,27].

In order to investigate the effect of MPCM concentration on the thermal properties of MPCM-GPC, The MPCM concentration was varied from 0 to 5.2 wt.% in steps of 2.6 wt.%. After mixing, MPCM-GPC were cast into molds at a size of 200 × 200 × 25 mm, and precured at room temperature for 24 h. The samples were then demolded and kept in water at room temperature for 28 days to reach a fully cured state. Finally, they were gently dried in an oven at 40 °C (to avoid shrinkage, thermal cracks, and broken microcapsules) until the sample weight remained unchanged [3].

2.2. Scanning electron microscopy

The fractured surfaces of MPCM-GPC samples containing 2.6 wt.% of MPCM were investigated using Zeiss EVO50 EP Scanning electron microscopy (Norway).

2.3. Density and porosity

The density and open porosity of the concrete samples were determined by EN 12390-7 (Eq. (1)) [28] and ASTM C1202-12 (Eq. (2)), respectively [29,30].

$$\rho = \frac{m_d}{V} \tag{1}$$

$$Open\ Porosity\ (\%) = \frac{m_s - m_d}{m_s - m_b} \times\ 100 \tag{2}$$

where ρ is the dry density of the sample, V is the volume of the sample, and m_d, m_b and m_s are oven-dried weight, the buoyant mass of the saturated sample in water and the mass of the saturated sample in air, respectively.

2.4. Thermal properties

A homemade guarded hot plates device [3,20,31] was designed to measure the thermal properties of concrete containing MPCM such as the thermal conductivity, the specific heat capacity and the heat storage capacity. The sample was placed in the middle of two aluminum plate heat exchangers. Each aluminum plate heat exchanger was connected to a programmable thermal regulated bath that defines the thermal conditions. A 40 mm thick polyethylene expanded foam (PEF) is used to cover the sample and minimize the heat losses from the sides of the samples. Accordingly,

Table 2
Composition of geopolymer concrete.

MPCM(wt.%)	Alkaline solution(g)	Water(g)	FA*(g)	GGBFS**(g)	Sand(g)	Aggregate(g)	Retarder(g)	MPCM(g)
0	200	50	300	200	871.8	851.7	5	0
2.6	200	50	300	200	696.9	851.7	5	63
5.2	200	50	300	200	522.7	851.7	5	117

(*) FA: Flyash (**) GGBFS: Ground granulated blast-furnace slag

the heat transfer through the sample can be assumed to behave according to one-dimensional thermal conditions. Calibrated heat flux sensors (Captecv, France) and calibrated T-type thermocouples (OMEGA, US) were utilized to record the temperature variations and heat fluxes through sample during testing.

Thermal conductivity

The thermal conductivity of the samples is defined according to the European standard EN-12667. The thermal conductivity of the samples in the liquid and solid states of PCM were determined by applying different temperature gradients between the top and bottom aluminum plate heat exchangers corresponding to a liquid state temperature range ($T > 30\,°C$) and a solid state temperature range ($T < 20\,°C$). After the samples reached a steady-state, the temperature and heat fluxes on both surfaces of the samples were collected. The thermal conductivity of the samples in the liquid and solid states of PCM was determined by [3]:

$$k = \frac{\varphi d}{\Delta T} \tag{3}$$

where $d = 25 \pm 1$ mm is the thickness of the sample, ΔT is the difference in temperature between the surfaces of the sample and φ is the average heat fluxes on both faces of the concrete sample.

Specific heat capacity/ heat storage capacity

The specific heat capacity of the concrete containing MPCM was determined by homogeneously raising the temperature of both aluminum plate heat exchangers from 5 °C and 45 °C at a heating rate of 10 °C/hour. It should be noted that a steady-state must be achieved at the initial and final temperatures of this process. The data including the heat flux (φ) and temperature (T) on both surfaces of the sample were collected during the process using calibrated heat flux sensors and calibrated thermocouples. The specific heat capacity as a function of temperature of the samples can be determined by [3,21]:

$$C_p(T) = \frac{A\varphi(T)}{m\frac{dT}{dt}} \tag{4}$$

The total heat storage capacity was calculated in the temperature range of 10–35 °C by Eq. (5) [21] using OriginPro 2016 Sr2.

$$Q = \frac{A}{m}\left(\int_{T1}^{T2} \varphi(T)dT\right) \tag{5}$$

where $T_1 = 10$ °C and $T_2 = 35$ °C. $A = 400$ cm^2 is the area of the sample.

In addition, the thermal conductivity and specific heat capacity of a homogeneous reference sample (granite rock-Nero Assoluto, Zimbabwe) were determined by using the homemade hot plate system and a TPS2500 hotdisk system (Lund) to evaluate the accuracy of the homemade system compared to the commercial one. The test was performed at room temperature ($\approx 20\,°C$) for the TPS2500 hotdisk system and a temperature range of 15–25 °C for the homemade system. The results are summarized in Table 3. There is a good agreement between the results measured by the homemade device and the TPS2500 with approximately 7% and 10% relative differences for the specific heat capacity and the thermal conductivity, respectively. In addition, the values are close to the litterature values of the specific heat capacity and thermal conductivity of granite rock (approximately 790 J/kg °C and 2.68–3.07 W/m °C [32]). Accordingly, the homemade sytem can be utilized to determine the thermal properties of building materials.

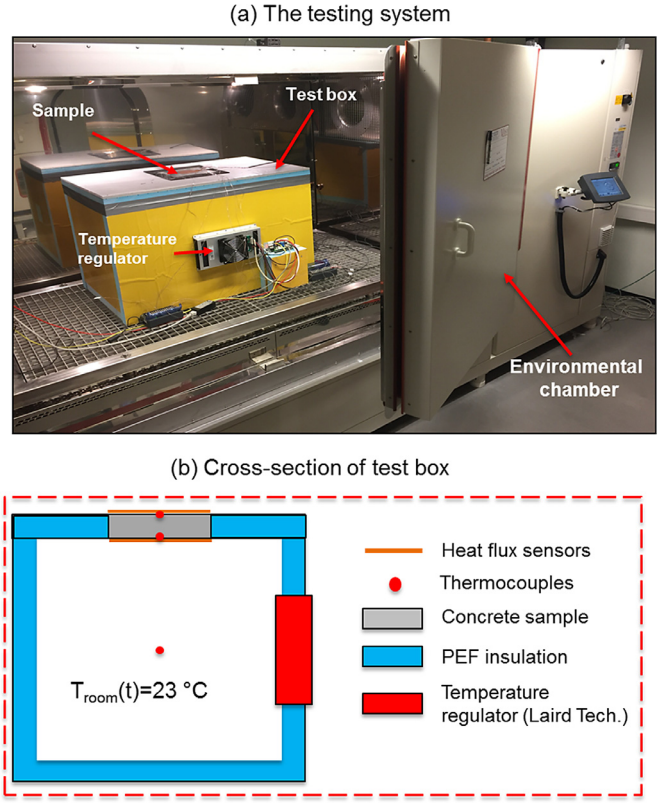

Fig. 1. The thermal performance testing system (a) test box placed in an environmental chamber, (b) sketch of the cross-section of the test box.

2.5. Energy saving aspects

Experimental test

Fig. 1 shows the thermal testing system which was utilized to investigate the thermal impact of geopolymer concrete containing microcapsules and to verify the numerical model. A small test box with inner dimensions of $600 \times 800 \times 600$ mm was made of 50 mm panels of polyethylene expanded foam (PEF) (Fig. 1) and was placed inside an environmental chamber to model outdoor temperature fluctuations. The concrete sample was placed in a rectangular opening (200×200 mm) in the middle of the top insulation panel.

For the test, the small test box was exposed to a daily sinusoidal temperature oscillation T_{out} (t) (Eq. (6)) using an environmental chamber (VT^3 4250, Vötsch, Germany) while the temperature inside the test box (T_{room}) was kept constant at 23 °C by a temperature regulator (AA150-Laird Technologies). For more information regarding the environmental chamber and temperature regulator, see the supporting document [33]. The maximum outdoor temperature T_{max} were set at 14:00 during the temperature

Table 3
Summarization of the specific heat capacity and thermal conductivity of granite rock determined by a homemade device and the TPS2500.

	Methods			Relative differences (%) $\frac{TPS2500-Homemade}{TPS2500} * 100\%$
	Homemade device	TPS2500	Literature	
Specific heat capacity (J/Kg °C)	704 ± 9	755	790	6.7
Thermal conductivity	2.65 ± 0.03	2.93	2.68–3.07	9.6

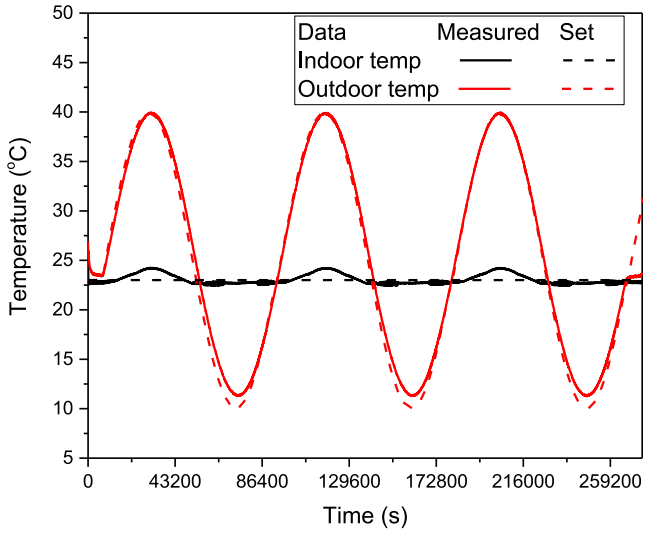

Fig. 2. The setting and measured temperatures of the indoor (inside text box) and outdoor (outside test box) environnments.

variation of the outdoor conditions:

$$T_{out}(t) = \frac{T_{max}+T_{min}}{2} + \frac{T_{max}-T_{min}}{2}\sin\left(\frac{\pi}{43200}t - \frac{2\pi}{3}\right) \quad (6)$$

where $T_{max} = 40$ °C and $T_{min} = 10$ °C are the maximum and minimum outdoor temperatures during one day, respectively. In order to simplify the thermal system, the effect of solar radiation is not considered. At the initial stage, both the indoor temperature (T_{room}) and outdoor temperature (T_{out}) were set at 23 °C for 2 h to reach a steady-state condition. Afterwards, the outdoor temperature cycles (Eq. (6)) were run continuously for 72 h.

Thermocouples were installed at different depths through the concrete wall in steps of 25 mm to measure the temperature across the samples. Heat flux sensors were installed on both surfaces of the concrete. Thermocouples were also placed at different positions both in the test box and in the environmental chamber to record the indoor temperature (T_{room}) and the outdoor temperature (T_{out}). All data were recorded every 60 s using a multichannel multimeter (LR8410-20 Hioki, Japan).

The outdoor and indoor temperatures during the experiments were recorded and is shown in Fig. 2. There is the slight mismatch between the setting temperature (Eq. (6)) and the mean collected temperature for both the outdoor and indoor temperature. This is more pronounced for the indoor temperature (T_{room}), which is probably due to the limits of the heating/cooling capacity of the temperature regulator. Therefore, the real experimental data collected using the calibrated thermal couples was utilized as input temperature data for the numerical calculation to improve the reality and accuracy of the method.

It is assumed that the insulation panels of the test box are perfectly thermally insulated. The heat will transfer to the test box via the concrete sample and be compensated for by the temperature regulator to maintain an inside temperature (T_{room}) of 23 °C. Accordingly, the total heat transfer to the test box can be calculated by Eq. (7) and corresponds to the energy (power consumption) of the temperature regulator (for heating when the temperature is below 23 °C and cooling when the temperature is higher than 23 °C):

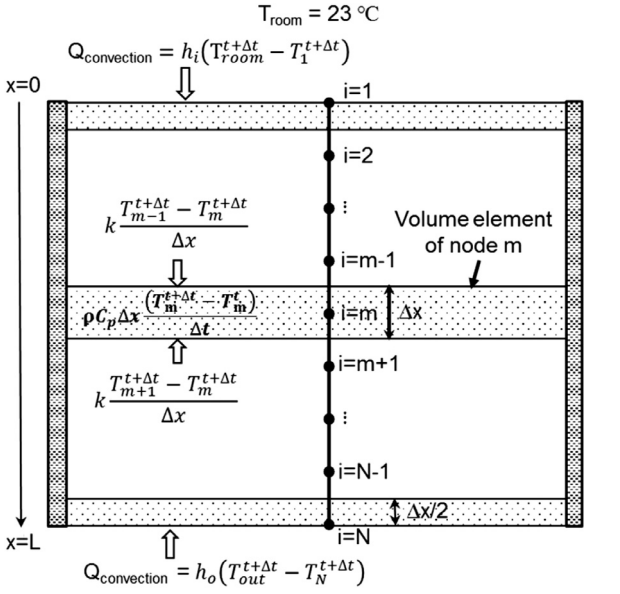

$$T_{out}(t) = \frac{T_{max}+T_{min}}{2} + \frac{T_{max}-T_{min}}{2}\sin(\frac{\pi}{43200}t - \frac{2\pi}{3})$$

Fig. 3. Schematic representation of the MPCM-concrete wall, and implicit finite differences method using the energy balance approach with boundary conditions. The energy balance states that heat transferred into the volume element from all of the surfaces is equal to the change in the energy content of the volume element during Δt [34].

$$P = \frac{\int_0^{24h} |\varphi_{indoor}| dt}{3600 \cdot 10^3} \quad (7)$$

where φ_{indoor} is the heat flux on the indoor side of the sample.

The power reduction Pr is defined as:

$$Pr = \frac{P_{GPC} - P_{MPCM-GPC}}{P_{GPC}} \cdot 100\% \quad (8)$$

where P_{GPC} and $P_{MPCM\text{-}GPC}$ are the power consumption of the heating/cooling system during 24 h for geopolymer concrete without and with MPCM, respectively.

2.6. Numerical method

A numerical model was developed to investigate the effect of MPCM addition on the thermal properties of a concrete wall. A simplified and uninsulated concrete wall was utilized. The thermal performance including the indoor surface temperature of the concrete wall, and the power consumption and power reduction for the heating and cooling system to maintain a constant indoor temperature were numerically calculated.

The model used to investigate the thermal behavior of the concrete wall is shown in Fig. 3. In order to simplify the model, it is assumed that:

- The heat transfer through the wall is a one-dimensional condition.
- The GPC containing microcapsules is homogeneous and isotropic.
- There is no heat generation in the samples.
- The convection effect in the melted PCM and super-cooling effects are neglectable.
- The indoor and outdoor heat transfer coefficients are assumed to be constant and are obtained from the literature.

The thermal conductivity, specific heat capacity, and density of the concrete walls which were used as input data for the numerical calculation were experimentally determined.

The mathematical model for one-dimensional heat transfer through the wall is [16,17,34]:

$$k\frac{\partial^2 T}{\partial x^2} = \rho C_p(T)\frac{\partial T}{\partial t} \tag{9}$$

where k, ρ, x are the thermal conductivity, density, and thickness of the wall, respectively. $C_p(T)$ is the specific heat capacity as a function of temperature of GPC containing microcapsules.

- **Numerical solution procedure**

The implicit finite difference method using the energy balance approach is used to solve the mathematic model and is illustrated in Fig. 3 [34]. The concrete wall is first discretized into a number of nodes (N) with a distance of Δx between two adjacent nodes. The volume elements over the nodes, where energy balance is applied, are formed to determine the temperatures at all nodes of the sample. The resulting implicit finite differences using the energy balance approach equations are:

- Interior node i = 1 (x = 0, indoor wall surface) (boundary condition [34]):

$$k\frac{T_2^{t+\Delta t} - T_1^{t+\Delta t}}{\Delta x} + h_i\left(T_{room}^{t+\Delta t} - T_1^{t+1\Delta t}\right) = \rho C_p\frac{\Delta x}{2}\frac{\left(T_1^{t+\Delta t} - T_1^{t}\right)}{\Delta t} \tag{10}$$

$$T_1^t = (1 + 2Bi_iFo)T_1^{t+\Delta t} - 2FoT_2^{t+\Delta t} - 2Bi_iFoT_{room}^{t+\Delta t} \tag{11}$$

- Inner node i = 2 to i = N-1

$$k\frac{T_{m-1}^{t+\Delta t} - T_m^{t+\Delta t}}{\Delta x} + k\frac{T_{m+1}^{t+\Delta t} - T_m^{t+\Delta t}}{\Delta x} = \rho C_p\Delta x\frac{T_m^{t+\Delta t} - T_m^{t}}{\Delta t} \tag{12}$$

$$T_m^t = -FoT_{m-1}^{t+\Delta t} + (1 + 2Fo)T_m^{t+\Delta t} - FoT_{m+1}^{t+\Delta t} \tag{13}$$

- Exterior node i = N (x = L, outdoor wall surface) (boundary condition [17,19,34,35]):

$$k\frac{T_{N-1}^{t+\Delta t} - T_N^{t+\Delta t}}{\Delta x} + h_o\left(T_{out}^{t+\Delta t} - T_N^{t+\Delta t}\right) = \rho C_p\frac{\Delta x}{2}\frac{\left(T_N^{t+\Delta t} - T_N^{t}\right)}{\Delta t} \tag{14}$$

$$T_N^t = -2FoT_{N-1}^{t+\Delta t} + (1 + 2\mathrm{Fo} + 2Bi_oFo)T_N^{t+1} - 2Bi_oFoT_{out}^{t+\Delta t} \tag{15}$$

where Bi_i and Bi_o are the Biot numbers in the room and in the outdoor environment, respectively:

$$Bi_i = \frac{h_i\Delta x}{k} \text{ and } Bi_o = \frac{h_o\Delta x}{k} \tag{16}$$

Fo is the Fourier number calculated as:

$$Fo = \frac{k\Delta t}{\rho C_p(\Delta x)^2} \tag{17}$$

T_m^t, $T_m^{t+\Delta t}$ are the temperatures of node m at time t and time $(t + \Delta t)$, respectively. In addition, $\Delta t = 60$ s and $\Delta x = 0.005$ m were selected for all cases. The initial temperature of the system was set to 23 °C. T_{out} and T_N are the outdoor temperature and the outdoor wall surface temperature (x = L). h_i and h_o are the indoor heat transfer coefficient (test box) and the outdoor heat transfer coefficient (environmental chamber), respectively. The heat transfer coefficient depends on the surface orientation, the direction of the heat flow and the velocity of the heat flow [36], which are collected from the experimental setup. To simplify the complex determination, the heat transfer coefficient values were selected from the literature based on the experimental setup information. Both h_i and h_o were considered to have the same value of 8 W/m^2 K for the horizontal wall. This is similar to the recommended values of ASHEA [36] and has been utilized for similar calculations previously [17,37,38].

MATLAB (Mathworks Inc., Natick, MA, USA) was employed to solve Eq. (10)Eq. (15) for all nodes. Relevant output data including the temperature across the thickness of the concrete samples, and the heat flux on the indoor surface (φ_{indoor}) were collected:

$$\varphi_{indoor}(t) = h_i\left(T_{room}^t - T_1^t\right) \tag{18}$$

Accordingly, the power required for a heating/cooling system to keep the indoor temperature stable was determined from Eq. (7) while the power reduction Pr was calculated from Eq. (8).

- **Testing conditions**

In order to evaluate the effect of microcapsules on the thermal impact on buildings using MPCM-GPC walls, various conditions were employed. Those conditions were carefully selected and applied on both the numerical model and the experimental tests.

- **Outdoor and indoor temperature**

In order to verify the numerical model, the actual outdoor temperature (environmental chamber) and indoor temperature (test box) were collected through the experiments using calibrated thermal couples. These data are utilized as the input temperature data for the numerical calculation to improve the reality and accuracy of the method.

- **MPCM concentration**

MPCM concentrations were selected at 0, 2.6 and 5.2 wt.% of the total weight of the concrete, to evaluate effect of MPCM concentration on the thermal performance of the concrete. The concentration of MPCM was limited to 5.2 wt.% since higher concentrations of MPCM resulted in a too low workability of the concrete.

- **Concrete thickness**

Due to the importance of the wall thickness on the heat transfer process of buildings, the thickness of the concrete walls was varied to investigate the effect on the thermal performance. GPC without microcapsules and GPC containing 5.2 wt.% microcapsules at thicknesses of 25, 50 and 75 mm were utilized.

3. Results and discussion

3.1. MPCM-GPC density and porosity

The open porosity of GPC as a function of MPCM concentration is shown in Fig. 4(a). The porosity increases when the MPCM concentration is raised. The smaller size of the microcapsules compared to the sand particles (see Fig. 1 in the supporting document [33]) is a possible explanation for this trend and in good agreement with previous findings [3]. The porosity of GPC containing PS-DVB/RT27 is lower than for MF/PCM24, especially after adding 2.6 wt.% microcapsules. MF/PCM24 has a polymer shell containing polar amine groups, which give rise to two opposite effects. Due

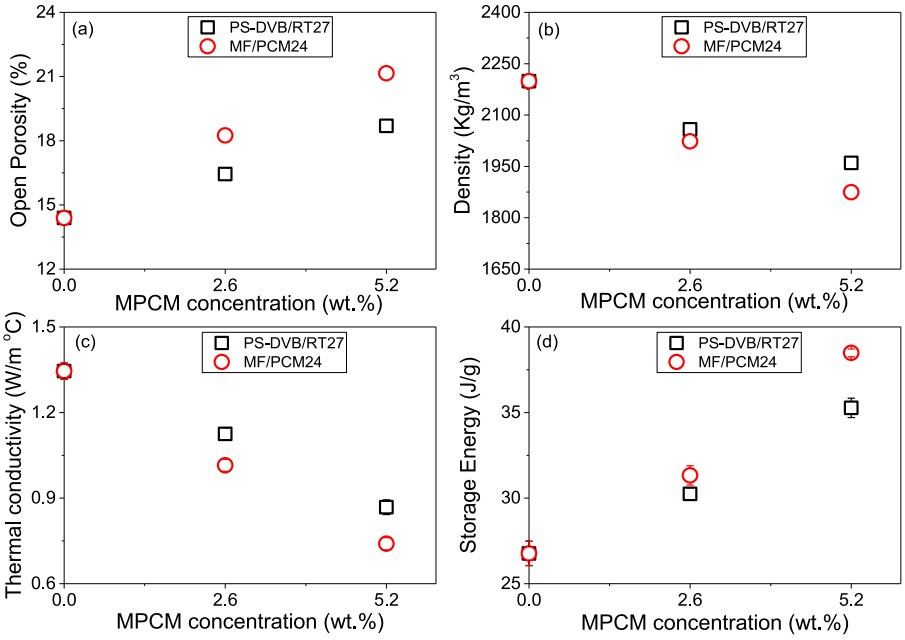

Fig. 4. (a) Open porosity, (b) density, (c) thermal conductivity and (d) storage energy as function of MPCM concentration of GPC containing PS-DVB/RT27 and GPC containing MF/PCM24.

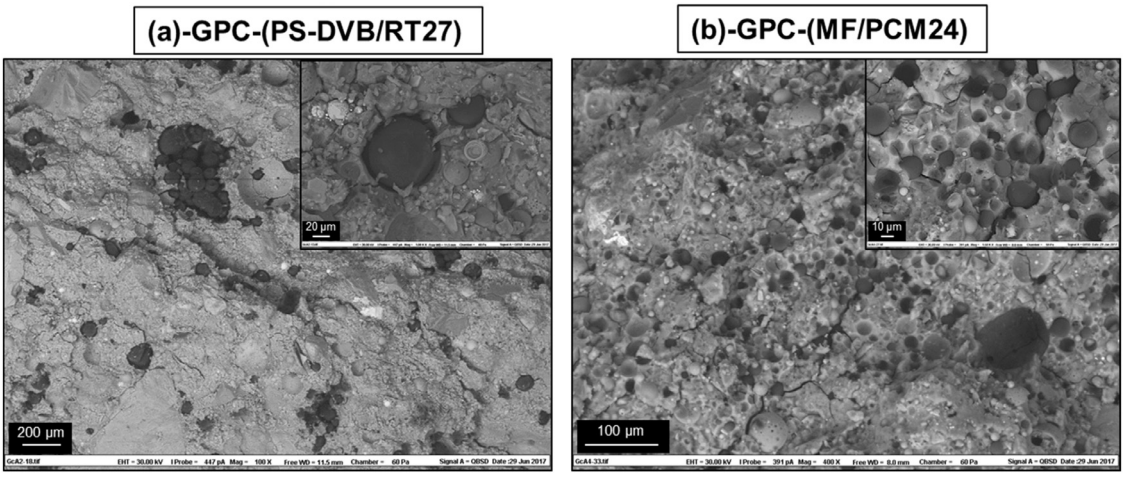

Fig. 5. SEM images of GPC containing 2.6 wt.% of (a) PS-DVB/RT27, (b) MF/PCM24.

to the polar groups, the polymer shell of MF/PCM24 is more compatible with the GPC. This causes better interface bonds between microcapsules and the geopolymer. This can reduce the air gaps between MPCM and GPC. PS-DVB/RT27 has a hydrophobic polymer shell which repel water. This causes more air gaps to be formed between the microcapsules and the GPC during the mixing process [3,39,40]. As is evident from the SEM images in Fig. 5, obvious gaps are observed between the concrete matrix and PS-DVB/RT27, while there is almost no air gaps between MF/PCM24 and the concrete matrix. This observation is supported by Zhang et al. [41] who concluded that the interface bonds between MPCM and Portland cement mortar can be improved by modifying the surface of the microcapsules using a silane coupling agent. On the other hand, the polar groups on the MF polymer shell and the smaller size of MF/PCM24 promotes adsorption of more water on the surface of the MF/PCM24 microcapsules [42]. This results in higher viscosities [3,5], which increases the probability of forming entrapped air voids during the mixing and pouring process. The higher porosity of GPC containing MF/PCM24 compared to GPC containing PS-DVB/RT27 is probably due to this effect.

The lower density of microcapsules compared to the sand it replaces and the increase of the porosity cause a decrease of the density of the MPCM-GPC samples when the MPCM concentration increases (Fig. 4(b)). Similar observations were also found previously [1,3]. The density decreases more for MF/PCM24, which has the highest porosity increase.

The average thermal conductivity of GPC containing different amounts of MPCM is summarized in Fig. 4(c). The thermal conductivity of MPCM-GPC decreases when the concentration of microcapsules is raised. This is due to the lower thermal conductivity of the microcapsules compared to that of replaced sand [3] and the enhanced porosity (Fig. 4(a)) after adding microcapsules. Furthermore, GPC containing MF/PCM24 has a lower thermal conductivity than GPC containing PS-DVB/RT27, which is in good agreement with the porosity data which rises faster for MF/PCM24 (Fig. 4(a)). Additionally, the better distribution of MF/PCM24 in the concrete matrix compared to PS-DVB/RT27 (Fig. 5) can provide an improved

thermal pathway through the concrete matrix and cause a lower thermal conductivity.

Fig. 4d summarizes the heat storage capacity of GPC as a function of microcapsule concentration within the temperature range of 10–35 °C. The heat storage capacity increases as more microcapsules are added to the concrete. This is in good agreement with Shadnia et al. [43] who demonstrated that the heat storage capacity of geopolymer mortar increases when the amount of MPCM increases. A similar observation has been observed for the integration of MPCM in Portland cement mortar [20,21], and Portland cement concrete [1,2]. In addition, the increase is more pronounced for MF/PCM24 due to the higher enthalpy of fusion (Table 1).

SEM images (Fig. 5) show that the microcapsules remain stable with a spherical shape in the concrete matrix. This demonstrates that both PS-DVB/RT27 and MF/PCM24 microcapsules have a good mechanical strength which can withstand the concrete mixing process. Hunger et al. [17] found that Micronal D5008X (polymethyl methacrylate/paraffin) MPCM was broken during the mixing process leading to a reduction of the Portland cement concrete compressive strength. Accordingly, both types of microcapsules utilized in the current study are probably stronger than the Micronal D5008X.

3.2. Specific heat capacity curve of MPCM-GPC

In order to accurately simulate the thermal performance of GPC containing MPCM, it is important to utilize an accurate equation to represent the experimental data of the specific heat capacity function ($C_p(T)$). This fitted $C_p(T)$ can be utilized for simulating the phase transition process.

Most previous studies define $C_p(T)$ assuming that the melting peak is symmetric, utilizing a piecewise function of temperature [16,17] or a Gaussian function of temperature [19] for modeling purposes. However, for concrete containing microcapsules this assumption is not in agreement with the experimental curve of $C_p(T)$, which presents an asymmetric shape of the melting peak [3,20–22]. We have therefore, utilized a new equation (Eq. (19)) based on the Pearson IV function to fit the specific heat capacity ($C_p(T)$) to the asymmetric shape:

$$Cp(T) = \begin{cases} Cp_o + h * \dfrac{w_l^{2m_l}}{\left(w_l^2 + \left(2^{\frac{1}{m_l}} - 1\right) * (2T - 2T_m)^2\right)^{m_l}} & for\ T \le T_m \\ Cp_o + h * \dfrac{w_r^{2m_r}}{\left(w_r^2 + \left(2^{\frac{1}{m_r}} - 1\right) * (2T - 2T_m)^2\right)^{m_r}} & for\ T > T_m \end{cases} \quad (19)$$

where Cp_o and h are the specific heat capacity outside the melting range and the height of the melting peak, respectively; T_m, w_l and w_r are the melting peak temperature, the phase change temperature range on the left side and right side of the melting peak, respectively; m_l and m_r are shape parameters for the left and right side of the peak, respectively.

The experimental data of the specific heat capacity versus temperature of GPC containing 5.2 wt.% microcapsules MF/PCM24 fitted to Eq. (19) is shown in Fig. 6(a). The high value of R^2 (0.99) and the non-systematic residuals (Fig. 6(b)) illustrate that this model is well suited for characterizing these systems.

Fig. 7 shows the fitted parameters obtained from Eq. (19). The specific heat capacity outside the melting range (Cp_o) of both GPC containing PS-DVB/RT27 and GPC containing MF/PCM24 increase when the concentration of microcapsules is raised (Fig. 7(a)). This is due to the higher specific heat capacity of the microcapsules compared to geopolymer concrete [3]. This is inconsistent with previous findings [3], where the specific heat capacity of MPCM-concrete remained almost unchanged after adding 2.7 wt.% of MPCM. The discrepancy is probably due to the higher microcapsule concentration applied in the current study (5.2 wt.%) which

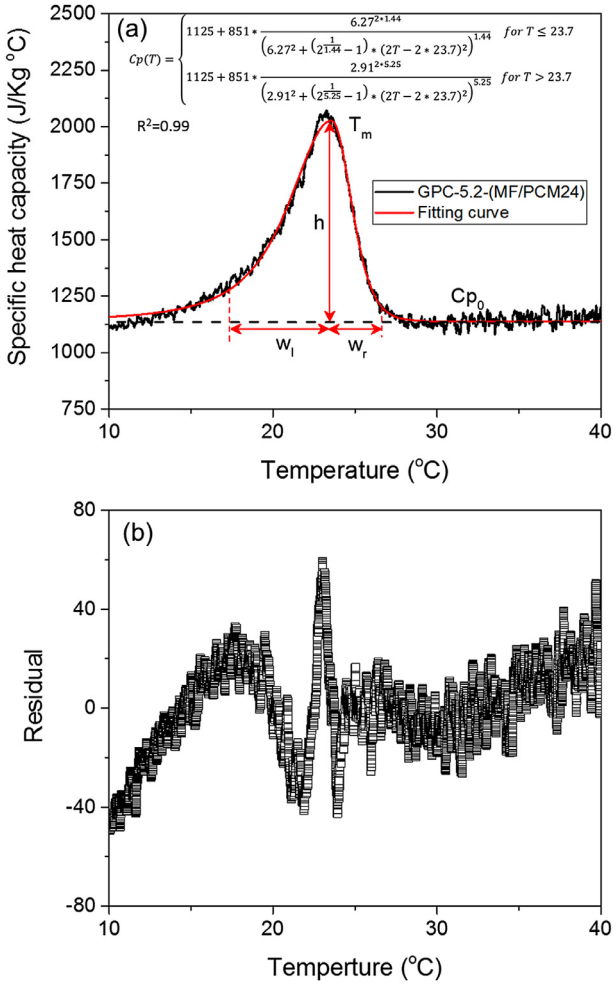

Fig. 6. (a) The specific heat capacity of GPC containing 5.2 wt.% of MF/PCM24 as function of temperature. The black solid line is experimental values. The red line shows the fitted values according to Eq. (19). (b) Residual plot between the measured and fitted values. (For interpretation of the references to color in this figure legend, the reader is referred to the web version of this article.)

is high enough to cause a significant increase of the specific heat capacity. This observation is in agreement with Joulin et al. [21], who studied effect of MPCM on the specific heat capacity of Portland cement mortar. Interestingly, the melting peak temperature of GPC containing microcapsules increases as the concentration of microcapsules is raised. The reason for this is unclear, but it might be caused by the reduced thermal conductivities of the samples (Fig. 4(c)) and the airgaps between the concrete matrix and the microcapsules (Fig. 5). When the thermal conductivity decreases it takes longer for the heat to reach the microcapsules to melt them, thereby shifting the melting peak to higher temperatures. In addition, the airgaps between PS-DVB/RT27 and the concrete matrix will act as an insulation layer, preventing the heat to efficiently reach the microcapsules. This will further delay the melting of the MPCM core.

3.3. Energy saving aspects

In order to evaluate the thermal impact of MPCM-concrete structures, numerical simulations and experimental measurements were carried out. The numerical model presented in this study is validated using the experimental results obtained by using the system show in Fig. 1. Results from the numerical model was compared with the experimental measurements.

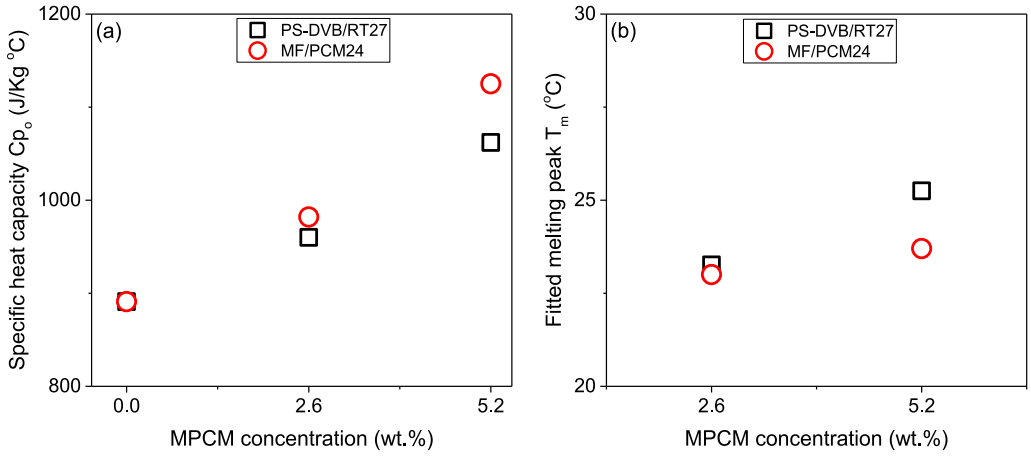

Fig. 7. (a) The specific heat capacity Cp_o and (b) the fitted melting peak T_m of GPC containing microcapsules as a function of microcapsule concentration obtained by fitting to Eq. (19).

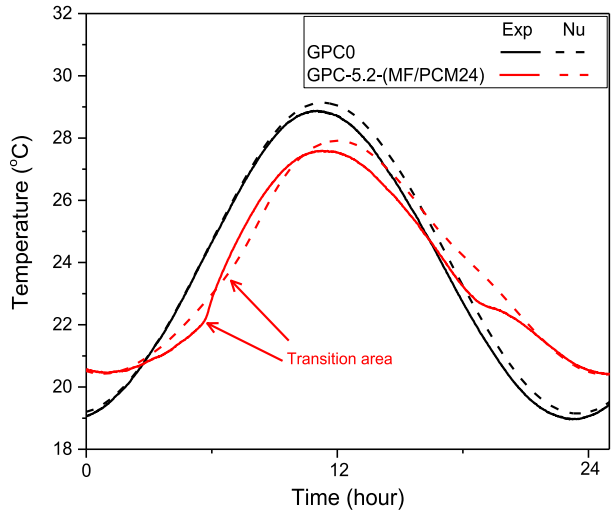

Fig. 8. Comparison of numerical model with experimental measurements for the indoor surface temperature of GPC0 and GPC-5.2-(MF/PCM24). The wall thickness of all samples is 75 mm.

Fig. 8 presents a comparison of the numerical model with experimental measurements for the indoor surface temperature of GPC0 and GPC-5.2-(MF/PCM24). There is a reasonable agreement between the experimental data and the numerical calculations. Both numerical and experimental data show that the variation of the indoor surface temperature of GPC containing 5.2 wt.% of MPCM is smaller than that of GPC without MPCM. This due to the higher heat storage capacity and lower thermal conductivity of GPC after the addition of MPCM. Accordingly, the integration of MPCM into the geopolymer concrete significantly reduce the influence of the outdoor temperature on the indoor surface temperature. This can be utilized to reduce the energy consumption for heating and cooling. However, the temperature peak occurs later in the numerical model than in the experimental work, and the melting transition is much clearer in the experimental data than in the numerical model (Fig. 8).

Fig. 9 shows a comparison of the numerical results with experimental measurements for the temperature variations across the concrete thickness at different times for GPC without MPCM and containing 5.2 wt.% of MPCM (PS-DVB/RT27 and MF/PCM24). For this test, the thermocouples were inserted through the 75 mm thick concrete sample with distance of 25 mm to determine the temperature across the concrete sample at different times (3 h, 6 h, 12 h and 22 h). Fig. 9 shows that the temperature across the thickness of the concrete obtained by experimental and numerical calculation exhibit the same trends for all samples. For GPC without MPCM (Fig. 9(a)) there is no significant deviation between the numerical model and the experimental data, illustrating that the numerical model provides a very good simulation at these conditions. In the presence of MPCM, there is a small deviation between the numerical model and the experimental data (<1 °C). This is probably due to the small deviations between the numerical calculations and the experimental data around the transition areas and the slightly different positions of the peaks (Fig. 8).

The heat flux on the indoor side of concrete samples were collected and compared to the numerical calculations. Fig. 10 shows the experimental curves and numerical curves of the heat flux on the indoor side of concrete wall without MPCM and containing 5.2 wt.% of MF/PCM24. For the GPC without MPCM there is a very good agreement between the simulation and the experimental data. In the presence of MPCM, the agreement is good except for a small deviation around the melting/solidifying transition points. The transition zones are more evident for the experimental data than in the simulations. There are several possible reasons for this discrepancy. The utilized model assumes a homogeneous sample, which is not strictly correct when microcapsules are distributed in the concrete matrix. In addition, the phase change process depends not only on temperature but also on the time it takes to completely convert the PCM to a liquid phase (melting process) or to a solid phase (solidifying process). Furthermore, the model does not take into account the effect of the interface between concrete and microcapsules, which can influence the heat transfer process especially when there are air gaps between the microcapsules and the concrete matrix. It is also possible that the heat capacity $C_p(T)$ utilized in the model is lower than the actual values and/or that the thermal conductivity is lower than expected.

The total heat transfer at the indoor surface can be used to determine the heat gain/loss toward the indoor environment. This must be compensated by a heating/cooling system in order to keep a constant indoor temperature. Accordingly, the total heat gain/loss toward the indoor environment can be considered as the energy consumption of the heating/cooling system to maintain a constant indoor temperature. In this study, the total energy consumption of the heating/cooling system is the sum of the heating power consumption when the indoor surface temperature $T_{x=0} < T_{room}$, and the cooling power consumption when the indoor surface temperature $T_{x=0} > T_{room}$. In order to verify the model, the simulated power consumption and power reduction were compared to exper-

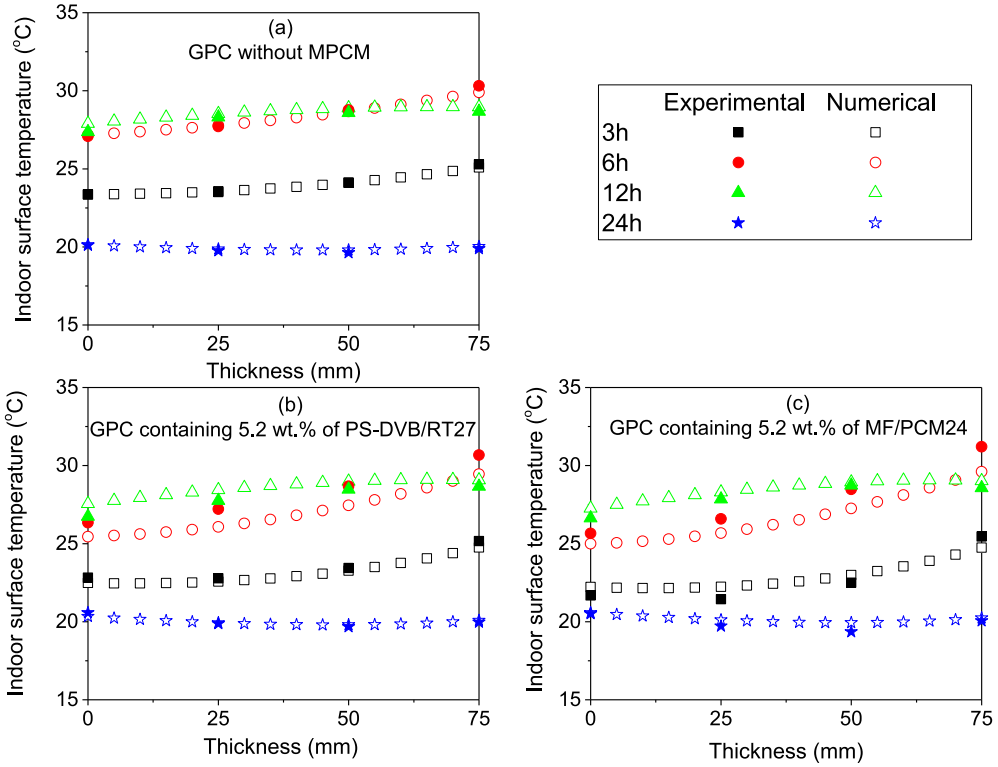

Fig. 9. Comparison of numerical model with experimental measurements for temperature variations across the concrete thickness at different times for (a) GPC0, (b) GPC-5.2-(PS-DVB/RT27) and (c) GPC-5.2-(MF/PCM24). The thickness of all samples is 75 mm.

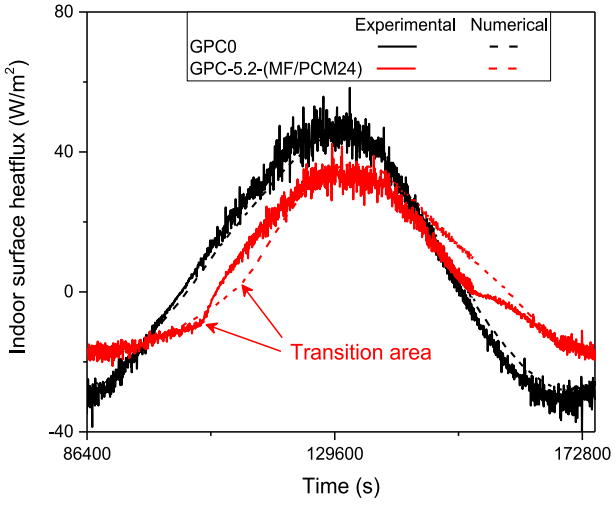

Fig. 10. Comparison of simulation model with experimental measurements for the indoor surface heat flux variations with time of GPC0 and GPC-5.2-(MF/PCM24). The thickness of all samples is 75 mm.

imental data. Furthermore, the effect of MPCM concentration, concrete wall thickness and different kinds of microcapsules on the thermal performance were investigated.

Fig. 11 presents the total calculated power consumption (Eq. (18)) and the power reduction (Eq. (19)) for the heating/cooling system to maintain an indoor temperature of 23 °C for both the experimental test and the numerical calculation. Two kinds of microcapsules PS-DVB/RT27 and MF/PCM24 were utilized. Fig. 11(a) reveals that the power consumption for the heating/cooling system to maintain an indoor temperature of 23 °C decreases substantially when the MPCM concentration is raised. The experimental data shows that the system can reduce the power consumption with up to 18.5% for PS-DVB/RT27 and 25.9% for MF/PCM24 after adding 5.2 wt.% of microcapsules (Fig. 11(b)). This demonstrates the promising thermal impact of GPC containing MPCM on the building envelope. The effect is due to a combination of a higher heat storage capacity and the better insulation properties of GPC after adding microcapsules. This is in agreement with previous experiments [1,3] and numerical calculations [17]. The simulations and experimental data exhibit the same trends. However, the simulations underestimate the amount of power that can be saved utilizing MPCM. This might be due to the deviations between the experimental and simulated data illustrated in Fig. 10. Furthermore, it is possible that the heat transfer coefficients for the indoor (h_i) and outdoor conditions (h_o) chosen from the literature might be higher than the actual values.

Fig. 12(a) shows the experimental curves of the indoor surface heat flux of GPC containing 5.2 wt.% of MF/PCM24 as a function of the concrete thickness. There is a reduction of the indoor surface heat flux when the wall becomes thicker. This is expected since the rate of heat conduction through the wall is inversely proportional to the wall thickness (Eq. (6)). This results in a lower power consumption to maintain the indoor temperature stable at 23 °C (Fig. 12(b)). Fig. 12(c) illustrates the power reduction of GPC containing 5.2 wt.% of microcapsules (GPC-5.2-(PS-DVB/RT27) and GPC-5.2-(MF/PCM24)) compared to corresponding samples without microcapsules as a function of concrete thickness (Eq. (19)). The experimental power reduction increase from 6.8% to 24.3% for GPC-5.2-(PS-DVB/RT27) and from 12.5% to 34.8% for GPC-5.2-(MF/PCM24) when the concrete thickness increases from 25 mm to 75 mm. This is probably due to a combination of the heat transfer reduction for the thicker samples and the effect of a high heat storage capacity after adding microcapsules.

GPC containing MF/PCM24 have a better thermal impact than GPC containing PS-DVB/RT27. This is expected since GPC with MF/PCM24 has lower thermal conductivity and higher heat storage

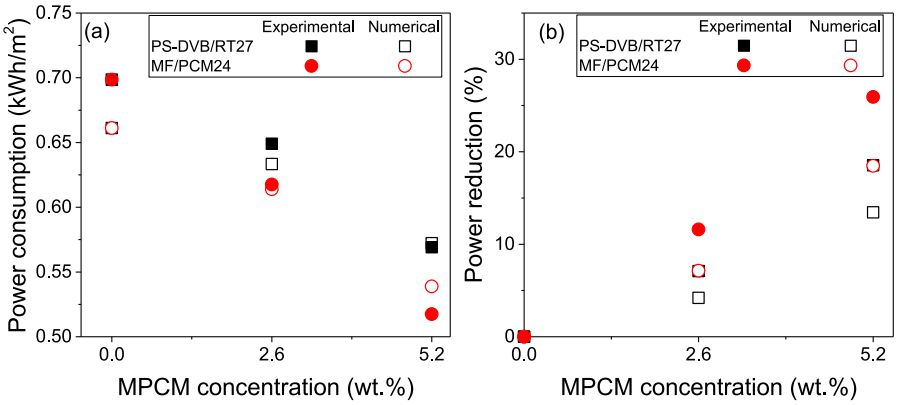

Fig. 11. Experimental data and simulation values of (a) the power consumption and (b) the power reduction of GPC as function of microcapsule concentration. Two kinds of microcapsules (PS-DVB/RT27 and MF/PCM24) were utilized. The thickness of the sample is 50 mm.

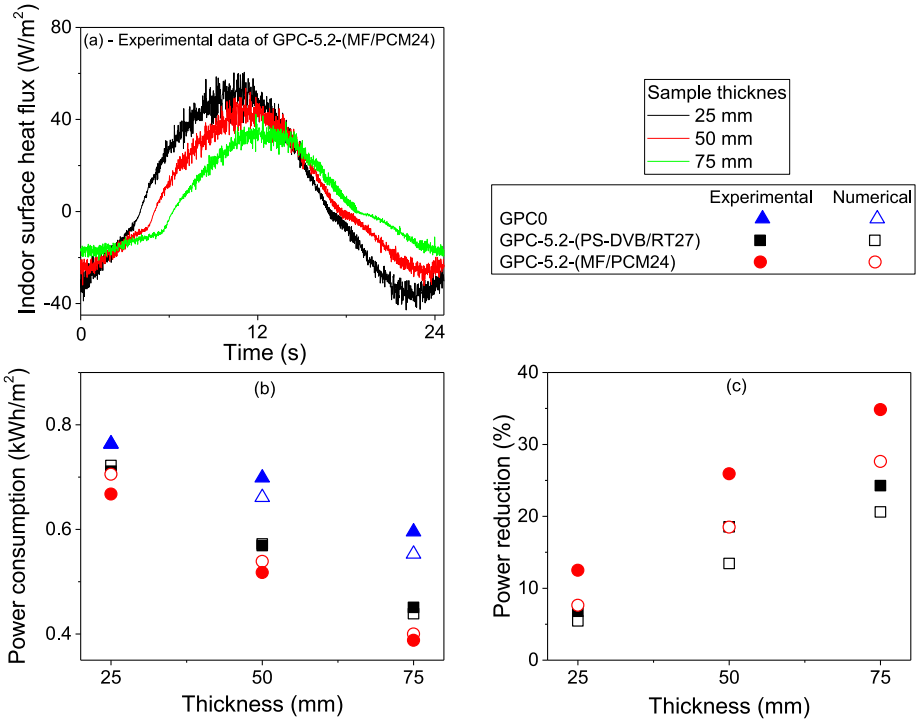

Fig. 12. The effect of wall thickness on (a) indoor surface heat flux GPC-5.2- (MF/PCM24), (b) the power consumption of GPC without microcapsules and GPC containing 5.2 wt.% microcapsules and (c) the power reduction of GPC containing 5.2 wt.% microcapsules compared to GPC without microcapsules.

capacity than that GPC containing PS-DVB/RT27 (Fig. 4). Although there are differences between the power consumption and power reduction between the experimental and numerical data, they exhibit the same trends.

The numerical model work well, with small deviations from the experimental data. Accordingly, this numerical model can be used as a quantitative tool to predict the thermal impact of concrete containing microcapsules at different climate conditions and for varying building designs.

4. Conclusion

Environmental friendly geopolymer concrete with a high thermal energy storage capacity containing microencapsulated phase change materials was achieved. By integrating microencapsulated phase change materials (MPCM) into geopolymer concrete (GPC), the thermal energy storage capacity of GPC is improved while the thermal conductivity and the density of geopolymer concrete (GPC) decrease. This results in an enhancement of the energy efficiency of the building envelope. A higher amount of MPCM in GPC or thicker MPCM-GPC walls can reduce the power consumption needed to stabilize the indoor temperature at 23 °C. The experimental data show that the power consumption can be reduced by up to 34.8% and 24.3% when utilizing a 75 mm concrete wall containing 5.2 wt.% of MF/PCM24 and PS-DVB/RT27, respectively.

The influence of the hygroscopic nature, the latent heat and the size distribution of microencapsulated phase change materials on the microstructure and thermal properties of geopolymer concrete (GPC) were explored. MF/PCM24 which has a polymer shell containing polar functional groups, a higher latent heat and small sizes (≈21 μm) exhibited a higher porosity, better interfacial bonds between microcapsules and the concrete matrix, a higher thermal energy storage capacity, and a lower thermal conductivity than PS-DVB/RT27, which has a hydrophobic polymer shell and larger sizes (≈130 μm).

Although there is a small deviation between numerical data and experimental results, the numerical values obtained for GPC containing MPCM was in good agreement with the experimental data. Accordingly, the numerical model, based on the implicit finite differences method using the energy balance approach and the heat capacity method, can be utilized to theoretically predict the thermal performance of building materials containing microencapsulated phase change materials. A new equation was successfully utilized to describe the specific heat capacity of GPC containing MPCM as function of temperature, which improved the accuracy of the numerical model.

Acknowledgments

We gratefully acknowledge funding from the Research Council of Norway, project number 238198. The authors gratefully acknowledge Rino Nilsen, Trond Atle Drøbak at Østfold University College, Prof. Lars Wadsö at Lund University and Van Thi Ai Nguyen for their assistance with laboratory work.

Supplementary materials

Supplementary material associated with this article can be found, in the online version, at doi:10.1016/j.enbuild.2018.06.011.

References

[1] A.G.E.M. Hunger, I. Mandilaras, H.J.H. Brouwers, M. Founti, The behavior of self-compacting concrete containing micro-encapsulated phase change materials, Cem. Concr. Compos. 31 (2009) 731–743.
[2] J.L.M. María Fenollera, ItziarI. Goicoechea, JaimeJ. Lorenzo, MiguelM. Ángel Álvarez, The influence of phase change materials on the properties of self-compacting concrete, Materials 6 (2013) 3530–3546.
[3] V.D. Cao, S. Pilehvar, C. Salas-Bringas, A.M. Szczotok, J.F. Rodriguez, M. Carmona, N. Al-Manasir, A.-L. Kjøniksen, Microencapsulated phase change materials for enhancing the thermal performance of Portland cement concrete and geopolymer concrete for passive building applications, Energy Convers. Manag. 133 (2017) 56–66.
[4] A. Eddhahak-Ouni, S. Drissi, J. Colin, J. Neji, S. Care, Experimental and multi-scale analysis of the thermal properties of Portland cement concretes embedded with microencapsulated phase change materials (PCMs), Appl. Therm. Eng. 64 (1–2) (2014) 32–39.
[5] S. Pilehvar, V.D. Cao, A.M. Szczotok, L. Valentini, D. Salvioni, M. Magistri, R. Pamies, A.-L. Kjøniksen, Mechanical properties and microscale changes of geopolymer concrete and Portland cement concrete containing micro-encapsulated phase change materials, Cem. Concr. Res. 100 (2017).
[6] A.L. Pisello, A. D'Alessandro, C. Fabiani, A.P. Fiorelli, F. Ubertini, L. F.Cabeza, A.L. Materazzi, Franco Cotana, Multifunctional analysis of innovative PCM-filled concretes, Energy Procedia 111 (2017) 81–90.
[7] Z. Wei, G. Falzone, B. Wang, A. Thiele, G. Puerta-Falla, L. Pilon, N. Neithalath, G. Sant, The durability of cementitious composites containing microencapsulated phase change materials, Cem. Concr. Compos. 81 (2017) 66–76.
[8] V.V. Rao, R. Parameshwaran, V.V. Ram, PCM-mortar based construction materials for energy efficient buildings: a review on research trends, Energy Build. 158 (2018) 95–122.
[9] S. Mengjie, N. Fuxin, M. Ning, H. Yanxin, D. Shiming, Review on building energy performance improvement using phase change materials, Energy Build. 158 (2018) 776–793.
[10] E. Benhelal, G. Zahedi, E. Shamsaei, A. Bahadori, Global strategies and potentials to curb CO2 emissions in cement industry, J. Cleaner Prod. 51 (2013) 142–161.
[11] P. Duxson, A. Fernandez-Jimenez, J.L. Provis, G.C. Lukey, A. Palomo, J.S.J.v, Deventer, Geopolymer technology: the current state of the art, J. Mater. Sci. 42 (2007) 2917–2933.
[12] Z. Zuhua, Y. Xiao, Z. Huajun, C. Yue, Role of water in the synthesis of calcined kaolin-based geopolymer, Appl. Clay Sci. 43 (2009) 218–223.
[13] S.N. AL-Saadi, Z.J. Zhai, Modeling phase change materials embedded in building enclosure: a review, Renew. Sustain. Energy Rev. 21 (2013) 659–673.
[14] J. Darkwa, O. Su, Thermal simulation of composite high conductivity laminated microencapsulated phase change material (MEPCM) board, Appl. Energy 95 (2012) 246–252.
[15] B.L. Gowreesunker, S.A. Tassou, M. Kolokotroni, Improved simulation of phase change processes in applications where conduction is the dominant heat transfer mode, Energy Build. 47 (2012) 353–359.
[16] P. Lamberg, R. Lehtiniemi, A.-M. Henell, Numerical and experimental investigation of melting and freezing processes in phase change material storage, Int. J. Therm. Sci. 43 (2004) 277–287.
[17] A.M. Thiele, G. Sant, L. Pilon, Diurnal thermal analysis of microencapsulated PCM-concrete composite walls, Energy Convers. Manag. 93 (2015) 215–227.
[18] A.M. Borreguero, M.L. Sánchez, J.L. Valverde, M. Carmona, J.F. Rodríguez, Thermal testing and numerical simulation of gypsum wallboards incorporated with different PCMs content, Appl. Energy 88 (2011) 930–937.
[19] B.M. Diaconu, M. Cruceru, Novel concept of composite phase change material wall system for year-round thermal energy savings, Energy Build. 42 (2010) 1759–1772.
[20] H. Cui, W. Liao, X. Mi, T.Y. Lo, D. Chen, Study on functional and mechanical properties of cement mortar withgraphite-modified microencapsulated phase-change materials, Energy Build. 105 (2015) 273–284.
[21] A. Joulin, L. Zalewski, S. Lassue, H. Naji, Experimental investigation of thermal characteristics of a mortar with or without a micro-encapsulated phase change material, Appl. Therm. Eng. 66 (2014) 171–180.
[22] M. Lachheba, M. Karkri, S.B. Nasrallah, Development and thermal characterization of an innovativegypsum-based composite incorporating phase change material asbuilding energy storage system, Energy Build. 107 (2015) 93–102.
[23] A.V. Sá, M. Azenha, H. de Sousa, A. Samagaio, Thermal enhancement of plastering mortars with phase change materials: experimental and numerical approach, Energy Build. 49 (2012) 16–27.
[24] M. Kheradmand, M. Azenha, J.L.B. de Aguiar, J. Castro-Gomes, Experimental and numerical studies of hybrid PCM embedded in plastering mortar for enhanced thermal behaviour of buildings, Energy 94 (2016) 250–261.
[25] A.M. Szczotok, M. Carmona, A.-L. Kjøniksen, J.F. Rodriguez, Equilibrium adsorption of polyvinylpyrrolidone and its role on thermoregulating microcapsules synthesis process, Colloid Polym. Sci. 40 (2017) 4061–4071.
[26] http://www.microteklabs.com/data-sheets.html, Data sheet of MPCM24D, in.
[27] S. Pilehvar, V.D. Cao, A.M. Szczotok, M. Carmona, R. Pamies, A.-L. Kjøniksen,
[28] Standard BS EN 12390-7. Testing hardened concrete, in: Part 7: Density of hardened concrete, 2009.
[29] M.Y.J. Liu, U.J. Alengaram, M.Z. Jumaat, K.H. Mo, Evaluation of thermal conductivity, mechanical and transportproperties of lightweight aggregate foamed geopolymer concrete, Energy Build. 72 (2014) 238–245.
[30] M. Safiuddin, N. Hearn, Comparison of ASTM saturation techniques for measuring the permeable porosity of concrete, Cem. Concr. Res. 35 (2005) 1008–1013.
[31] P. Tittelein, S. Gibout, E. Franquet, K. Johannes, L. Zalewski, F. Kuznik, J.-P. Dumas, S. Lassue, J.-P. Bédécarrats, D. David, Simulation of the thermal and energy behaviour of a composite material containing encapsulated-PCM: influence of the thermodynamical modelling, Appl. Energy 140 (2015) 269–274.
[32] E. Lev, I. Kutasov, A. Pilchin, Applied Geothermics, Springer-Verlag Berlin Heidelberg, 2014.
[33] V.D. Cao, S. Pilehvar, C. Salas-Bringas, A.M. Szczotok, T.Q. Bui, M. Carmona, J.F. Rodriguez, A.-L. Kjøniksen, Thermal performance and numerical simulation of geopolymer concrete containing different types of thermoregulating materials for passive building applications, Energy and Buildings.
[34] Y.A. Cengel, Heat Transfer: A Practical Approach, 2nd ed., Mcgraw-Hill, 2002.
[35] L.A.A. Pasupathy, R. Velraj, R.V. Seeniraj, Experimental investigation and numerical simulation analysis on the thermal performance of a building roof incorporating phase change material (PCM) for thermal management, Appl. Therm. Eng. 28 (2008) 556–565.
[36] ASHRAE, Handbook of Fundamentals, American Society of Heating, Refrigerating and Air-Conditioning Engineers, Inc., Atlanta, 2013.
[37] E.M. Alawadhi, Thermal analysis of a building brick containing phase change material, Energy Build. 40 (3) (2008) 351–357.
[38] S.A. Al-Sanea, Thermal performance of building roof elements, Build. Environ. 37 (2002) 665–675.
[39] D. Fedroff, S. Ahmad, B. Savas, Mechanical properties of concrete with ground waste tire rubber, Transp. Res. Board 1532 (1996) 66–72.
[40] Z.K. Khatib, F.M. Bayomy, Rubberized portland cement concrete, J. Mater. Civil Eng. 11 (1999) 206–213.
[41] J. Zhang, H. Yan, S.L. Chen, X.M. Wang, Z.D. Gu, The preparation and properties of the low melting point microencapsulated paraffin insulation mortar, Appl. Mech. Mater. 71-78 (2011) 4835–4838.
[42] V.D. Cao, S. Pilehvar, C. Salas-Bringas, A.M. Szczotok, L. Valentini, M. Carmona, J.F. Rodriguez, A.-L. Kjøniksen, Influence of microcapsule size and shell polarity on thermal and mechanical properties of thermoregulating geopolymer concrete for passive building applications, Energy Convers. Manag. 164 (2018) 198–209.
[43] R. Shadnia, L. Zhang, P. Li, Experimental study of geopolymer mortar with incorporated PCM, Constr. Build. Mater. 84 (2015) 95–102.